

# Highly grafted polystyrene/polyvinylpyridine polymer gold nanoparticles in a good solvent: effects of chain length and composition†

Zbyšek Posel,<sup>‡,ab</sup> Paola Posocco,<sup>‡,cd</sup> Martin Lísal,<sup>be</sup> Maurizio Fermeglia<sup>cd</sup> and Sabrina Pricl<sup>\*cd</sup>

In this work, the structural features of spherical gold nanoparticles (NPs) decorated with highly grafted poly(styrene) (PS), poly(vinylpyridine) (PVP) and PS–PVP diblock copolymer brushes immersed in a good solvent are investigated by means of Dissipative Particle Dynamics (DPD) simulations as a function of grafted chain length and of homopolymer and copolymer chain composition. For NPs grafted either by PS or PVP homopolymer brushes (selected as a proof of concept), good agreement between the Daoud–Cotton theory, experimental evidence, and our DPD simulations is observed in the scaling behavior of single chain properties, especially for longer grafted chains, and in brush thickness prediction. On the other hand, for grafted chain lengths comparable to NP dimensions parabolic-like profiles of the end-monomer distributions are obtained. Furthermore, a region of high concentration of polymer segments is observed in the monomer density distribution for long homopolymers. In the case of copolymer-decorated NPs, the repulsion between PS and PVP blocks is found to substantially influence the radius of gyration and the shape of the end-monomer distribution of the relevant polymer shell. Moreover, for diblock chains, the un-swollen region is observed to be thinner (and, correspondingly, the swollen layer thicker) than that of a NP modified with a homopolymer of the same length. Finally, the lateral segregation of PS and PVP blocks is evidenced by our calculations and a detailed analysis of the corona behavior is reported, thus revealing the key parameters in controlling the surface properties and the response of diblock copolymer modified nanoparticles.

Accepted 3rd March 2016

## Introduction

Polymer brushes composed of flexible polymer chains tethered to solid substrates are widely used to tailor surfaces for specific applications.<sup>1,2</sup> Spherical polymer brushes can be formed from macromolecules anchored *via* a special end group to *e.g.*, the spherical inorganic nanoparticle (NP) surface and extending outward into the surrounding medium. These systems are

prototypical examples of “hairy polymer nano-objects”,<sup>3,4</sup> which are of great actual interest in a variety of advanced technological fields such as colloid stabilization,<sup>5</sup> building blocks for nanostructured materials and nanocomposites,<sup>6,7</sup> and medical and biological applications,<sup>8,9</sup> just to mention a few. In addition, the recent development of precise synthetic pathways has led to the production of NPs decorated with brushes of very high grafting density, thereby expanding the application range of these functional nanomaterials even further.<sup>4,10,11</sup>

While a classical polymer nanocomposite is a blend of inorganic nanoparticles and a polymer matrix, hairy polymer nanoparticles (HPNs) represent single-component objects with an organic component linked directly to the inorganic core. Thus, the architecture of HPNs is designed to overcome classical “mixing and stability problems” commonly present in polymer nanocomposites. Therefore, the possibility to use assemblies of HPNs in solvent or in solvent-free systems has enormously attracted researchers’ interest.<sup>12–14</sup>

Experimental and computational studies of homopolymer functionalized NPs in the polymer matrix, solvent, and melt have clearly shown that the properties of these NPs can be

<sup>a</sup> Department of Informatics, Faculty of Science, J. E. Purkinje University, Ústí nad Labem, Czech Republic

<sup>b</sup> Laboratory of Physics and Chemistry of Aerosols, Institute of Chemical Process Fundamentals of the CAS, v. v. i., Prague, Czech Republic

<sup>c</sup> Molecular Simulations Engineering (MOSE) Laboratory, Department of Engineering and Architecture (DEA), University of Trieste, via Valerio 10, 34127 Trieste, Italy

<sup>d</sup> National Interuniversity Consortium for Material Science and Technology (INSTM), Research Unit MOSE-DEA, University of Trieste, Italy.  
E-mail: sabrina.pricl@di3.units.it

<sup>e</sup> Department of Physics, Faculty of Science, J. E. Purkinje University, Ústí nad Labem, Czech Republic

† Electronic supplementary information (ESI) available. See DOI: 10.1039/c5sm02867a

‡ ZP and PP equally contributed to this work.

tailored by modulating molecular parameters such as grafting density,<sup>15</sup> NP size,<sup>16</sup> graft placement,<sup>17</sup> graft and matrix molecular weight,<sup>18</sup> and NP shape.<sup>19</sup> At the same time, NP copolymer functionalization, as opposed to homopolymer functionalization, constitutes an additional tuning parameter of the grafted sequence and monomer chemistry (or interactions), which provides further control over the behavior of the polymer grafted nanoparticles.

When one considers the processing of spherical polymer brushes in the context of any of the applications mentioned above, understanding their structure and properties in solvents of various quality is of fundamental interest.<sup>3</sup> Unfortunately, however, the rational design of interface- or surface-active polymer modifiers still lacks crucial molecular scale information about the behavior and structure–property relationships of the brushes. This is especially true in the regime of dense brushes, since high grafting densities are potentially outside the limits of classical polymer brush theory. Thus, for instance, the known Daoud–Cotton (DC) theory<sup>20</sup> describing star polymers can be applied only to some extent to long brushes tethered to spherical surfaces. Therefore, computer simulations are to be employed to gain a general theoretical understanding of hairy polymer nano-objects at the molecular level. Indeed, a number of studies have appeared dealing with molecular simulations of these systems at the atomistic level, although they mainly involved short oligomer-like chains or low grafting densities.<sup>21,22</sup>

The structure and scaling behavior of spherical brushes have been studied also on larger scales (*i.e.*, coarse-graining), where the chemical specificity is lost. Thus, using a classical bead-spring model, Binder<sup>23</sup> and his group studied the scaling behavior of spherical brushes in the implicit solvent. Among other things, they showed that chains with a size comparable to NP dimensions exhibit a parabolic decay in monomer density distribution and that chain ends are distributed through the whole polymer shell rather than being located only at the edge. Also, they observed a broad crossover between scaling of the brush height on the flat and curved surface. Their results were compared against the Daoud–Cotton model with good agreement in scaling behavior. In addition, the same bead-spring model was used to study the effect of solvent quality on the rearrangement of grafted chains on spherical surfaces.<sup>24</sup> The effect of the monomer sequence on the arrangement of copolymer chains grafted to spherical surfaces was investigated in another study by means of lattice Monte Carlo simulations.<sup>25,26</sup> It was shown that the chain architecture (*i.e.*, monomer sequence) influences chain aggregation on the spherical surface. Specifically, an alternating sequence of monomers prevents further assembling into larger structures whereas diblock sequences allow the aggregation of same species into larger clusters under certain conditions. Nevertheless, the adoption of lattice-based models of spherical brushes cannot be extended to the case of high grafting densities.

In addition, several attempts were made to apply mesoscale models – and specifically Dissipative Particle Dynamics (DPD) – to flat brushes or to polymer protected nanoparticles.<sup>27,28</sup> Such studies were very valuable for deriving general dependencies of

brush characteristics on grafting density or chain length, but for direct comparison to experimental data more specific models are needed.

Accordingly, in this paper we adopted a promising, alternative route towards coarse-grain polymer-grafted NPs, which retains the fundamental chemical details while taking advantage of mesoscopic simulations at the same time. Specifically, we present here the application of our mesoscale approach to linear poly(styrene) (PS)/poly(vinylpyridine) (PVP) homopolymer and copolymer chains tethered onto a spherical gold NPs in the experimentally highly dense polymer regime (1 chain per nm<sup>2</sup>) and good solvent environment. We then analyze and discuss the structural and scaling behavior of the PS/PVP grafted chains with specific attention to the effect of chain length and composition. In this respect, the polymer density profiles around the NPs and the static properties of the grafted chains are examined. Based on these data, the brush thickness of the grafted chains is estimated and its scaling behavior is compared against theoretical models and experimental data, when available.

## Models and computational details

Dissipative Particle Dynamics (DPD)<sup>29,30</sup> simulations have been proved to be an effective tool for modelling structural phenomena like the self-assembly of diblock copolymers in melt and in solution,<sup>31,32</sup> polymer nanocomposites,<sup>33–35</sup> and membranes<sup>36</sup> under various solvent conditions, just to mention a few. In a DPD simulation,<sup>30,37</sup> the actual material (solvents, nanoparticles or polymer chains) is modeled as a collection of spherical particles that represent lumps of the material. DPD particles are defined by mass  $m_i$ , position  $r_i$ , and velocity  $v_i$ , and interact with each other *via* a total force  $F$  that is the sum of a conservative force  $F^C$ , a dissipative force  $F^D$ , and a random force  $F^R$ :

$$F = F^C + F^D + F^R \quad (1)$$

$F^C$  typically includes non-bonded interaction between beads  $i$  and  $j$ :

$$F^C(r_{ij}) = \begin{cases} a_{ij}(1 - r_{ij}/r_c)r_{ij} & r_{ij} < r_c \\ 0 & r_{ij} \geq r_c \end{cases} \quad (2)$$

where  $a_{ij}$  and  $r_{ij} = r_j - r_i$  are the maximum repulsion and the separation vector between particles  $i$  and  $j$ , respectively, while  $r_c$  is the cut-off distance at which the influence of  $F^C$  vanishes.

The remaining two forces,  $F^D$  and  $F^R$ , which arise from degrees of freedom neglected by coarse-graining, are given by:

$$F^D = -\gamma_{ij}\omega^D(r_{ij})\left(\frac{r_{ij}}{r_{ij}} \cdot v_{ij}\right)\frac{r_{ij}}{r_{ij}} \quad (3)$$

$$F^R = \sigma_{ij}\omega^R(r_{ij})\frac{\xi_{ij}}{\sqrt{\Delta t}}\frac{r_{ij}}{r_{ij}} \quad (4)$$

where  $\omega^D(r_{ij})$  and  $\omega^R(r_{ij})$  are weight functions that vanish for  $r_{ij} \geq r_c$ ,  $\gamma_{ij}$  is the friction coefficient,  $\sigma_{ij}$  is the noise amplitude,  $v_{ij} = v_i - v_j$  is the velocity vector,  $\xi_{ij} = \xi_{ji}$  is a Gaussian random

number with zero mean and unit variance that is chosen independently for each pair of interacting particles, and  $\Delta t$  is the time step. The pair-wise dissipative and random forces guarantee that the momentum is locally conserved and this, in turn, ensures correct hydrodynamic behavior.

Español and Warren<sup>38</sup> showed that a DPD system samples the canonical ensemble and obeys the fluctuation-dissipation theorem if the following relationships hold:

$$\omega^D(r_{ij}) = [\omega^R(r_{ij})]^2 \quad (5)$$

$$\sigma_{ij}^2 = 2\gamma_{ij}k_B T \quad (6)$$

where  $k_B$  is the Boltzmann constant and  $T$  is the equilibrium temperature.

$\omega^D(r_{ij})$  and  $\omega^R(r_{ij})$  are typically chosen<sup>29</sup> as:

$$\omega^D(r_{ij}) = [\omega^R(r_{ij})]^2 = \begin{cases} \left(1 - \frac{r_{ij}}{r_c}\right)^2 & (r_{ij} < r_c) \\ 0 & (r_{ij} \geq r_c) \end{cases} \quad (7)$$

Finally, when modeling chains, another force is active in the system, *i.e.*, a harmonic spring connecting two adjacent particles  $i$  and  $j$ :

$$F^S = K_b(r_{ij} - r_0)\frac{r_{ij}}{r_{ij}} \quad (8)$$

where  $K_b$  is the spring stiffness and  $r_0$  is the equilibrium distance between the particles.

### Polymer-grafted nanoparticle mesoscopic model

Our computational efforts were devoted to modelling spherical Au NPs grafted by PS, PVP or PVP-PS diblock copolymer (DBC) chains. In previous experimental studies reported by Kramer *et al.*<sup>39</sup> gold NPs coated by PS chains of different molecular weights  $M_n$  ( $M_n = 1500$ – $13\,000$  Da) with areal chain densities (or grafting density)  $\sigma$  ranging from 0.32 to 1.64 chains per nm<sup>2</sup> were synthesized and characterized. The gold core diameter was approximately in the range of 2–5 nm. Accordingly, in an attempt to map our models onto these experimental systems, we set a NP core diameter of 3 nm and a grafting density  $\sigma = 1$  chain per nm<sup>2</sup> (laying in the high regime of  $\sigma$  experimentally feasible for PS-*b*-PVP modified Au NPs<sup>39</sup>) and varied the grafted chain length in the range of 3000–18 000 Da. Thus, the total number of grafted chains  $G$  was obtained to be  $G = 4\pi r_s^2 \sigma \approx 28.3$  which is approximately 28 chains, with  $r_s$  being the radius of the spherical NP.

Au NPs were modeled at the coarse-grained level as a collection of Au DPD beads connected by a stiff harmonic spring to preserve the NP shape, whereas each polymer chain was represented by a flexible chain model of beads connected by harmonic springs  $K_b$ . Tetrahydrofuran (THF), modeled as a single bead, was selected as a good solvent for these decorated NP systems.<sup>39</sup>

Each DPD bead in a polymer chain represents a statistical distribution of PVP or PS monomers. In previous papers<sup>40–42</sup> we showed that the characteristic ratio  $C_\infty$  (*i.e.*, the ratio of the mean square unperturbed end-to-end distance for the chain to

the value expected for a freely jointed chain with the same number of bonds) is a reliable parameter for mapping the structure of PVP and PS polymers onto a flexible chain model; accordingly, here we used the same statistical approach. However, at variance with our previous work, where we mapped one single chain length, here we averaged the  $C_\infty$  of the shortest and longest polymer chains considered to estimate the corresponding cut-off distance  $r_c = 1.41$  nm. When flexible macromolecules are modeled as Gaussian chains,  $C_\infty$  represents also the number of monomers making up a Kuhn segment (*i.e.*, contained in a single DPD bead, 6.5 in the present case). Therefore, the bead volume  $V_{\text{DPD}}$  can be simply obtained by multiplying the characteristic ratio by the molecular monomer volume; then, the cut-off distance  $r_c$  can be easily derived from the relation  $r_c = (\rho V_{\text{DPD}})^{1/3}$ , where  $\rho$  is the reduced density usually set to 3.<sup>29</sup>

As a consequence, real polymers with  $M_n = 1500$ – $13\,000$  Da were modeled by chains with  $N = \{4, 8, 12, 16, 20, 24, 28\}$  DPD beads per grafted chain. For DBC chains, the total chain length is expressed as  $N = n + m$ , where  $n$  and  $m$  are the lengths of the PVP and PS block, respectively. To evaluate the effect of the DBC chain architecture, for each total chain length  $N$  we considered different relative compositions of each block, defined as  $f_{\text{PVP}} = n/(n + m)$  and, correspondingly,  $f_{\text{PS}} = 1 - f_{\text{PVP}}$ . Table 1 summarizes all systems studied in this work.

**Table 1** Summary of the systems studied in this work.  $N$  is the total chain length,  $n$  is number of PVP DPD beads,  $m$  is the number of PS DPD beads, and  $f_{\text{PVP}}$  is the relative composition of the PVP block

	$n$	$m$	$f_{\text{PVP}}$	$n$	$m$	$f_{\text{PVP}}$	
$N = 28$	0	28	0.0	$N = 24$	0	24	0.0
	14	14	0.5		12	12	0.5
	28	0	1.0		24	0	1.0
$N = 20$	0	20	0.0	$N = 16$	0	16	0.00
	2	18	0.1		2	14	0.13
	4	16	0.2		3	13	0.19
	6	14	0.3		5	11	0.31
	8	12	0.4		6	10	0.37
	10	10	0.5		8	8	0.50
	12	8	0.6		10	6	0.63
	14	6	0.7		11	5	0.69
	16	4	0.8		13	3	0.81
	18	2	0.9		14	2	0.87
	20	0	1.0		16	0	1.00
$N = 12$	0	12	0.00	$N = 8$	0	8	0.00
	1	11	0.08		1	7	0.13
	2	10	0.16		2	6	0.25
	4	8	0.33		3	5	0.38
	5	7	0.42		4	4	0.50
	6	6	0.50		5	3	0.62
	7	5	0.58		6	2	0.75
	8	4	0.67		7	1	0.87
	10	2	0.84		8	0	1.00
	11	1	0.92				
	12	0	1.00				
$N = 4$	0	4	0.00				
	1	3	0.25				
	2	2	0.50				
	3	1	0.75				
	4	0	1.00				

During simulation, the spherical shape of gold NPs was preserved by adopting a high spring stiffness, *i.e.*,  $K_b = 200k_B T$  (where  $k_B$  is Boltzmann’s constant and  $T$  is the temperature). Each Au bead was bonded to Au beads falling within a bonding radius  $r_b$ ; accordingly, each pair of Au beads has a unique equilibrium distance of the spring bond.

The same  $K_b$  value was used to bond the first polymer bead to the NP surface, the equilibrium distance being set to  $r_0 = 0.5r_c$ . Finally, polymer chain beads were bonded with harmonic spring  $K_b = 4k_B T$  and equilibrium distance  $r_0 = 0$ .

Once the mesoscale architecture of each system component was established as described above, the underlying chemistry of each DPD system component was accounted for by intra- and inter-molecular interactions between the DPD segments. The DPD  $a_{ij}$  parameters were derived following the procedure outlined in our previous studies<sup>40,41</sup> and briefly summarized here. For polymer–polymer interactions, we applied the relationship proposed by Glotzer and her group<sup>43</sup> for block copolymers:

$$\frac{a_{ij}r_c}{k_B T} = \frac{a_{ii}r_c}{k_B T} + 3.27 \left( 1 + \frac{3.9}{N^{0.51}} \right) \chi_{ij} \quad (9)$$

where  $\chi_{ij}$  is the commonly used Flory–Huggins interaction parameter<sup>29</sup> between polymer segments,  $N$  is the total length of the flexible chain,  $k_B$  is the Boltzmann constant and  $T$  the equilibrium temperature. Solvent–polymer mesoscale interactions were derived from the commonly used equation proposed by Groot<sup>29</sup>  $a_{ij} = a_{ii} + 3.27\chi_{ij}$ , where  $a_{PS-PS} = 25$  was selected as the reference base (as in eqn (9)).  $\chi_{ij}$  is defined in terms of the solubility parameters of the  $i$  and  $j$  components as:

$$\chi_{ij} = \frac{V_{\text{DPD}}}{k_B T} (\delta_i - \delta_j)^2 \quad (10)$$

where  $V_{\text{DPD}}$  is the volume of DPD bead and  $\delta_i$  is the solubility parameters of the  $i$ -th component, which is in turn related to the cohesive energy density  $e_{\text{coh}}$  by:

$$\delta = \sqrt{\frac{E_{\text{coh}}}{V}} = \sqrt{e_{\text{coh}}} \quad (11)$$

in which  $E_{\text{coh}}$  is the cohesive energy of the  $i$ -th component and  $V$  is its molar volume at a given temperature. The value of  $E_{\text{coh}}$  for, *e.g.*, THF can be derived from canonical ( $NVT$ ) ensemble MD simulation by calculating the difference between the non-bonded component of the potential energy of a three-dimensional (3D) periodic structure and the corresponding value for an isolated parent chain *in a vacuum*.

All hard–soft interactions (*i.e.*, interactions involving THF and gold NP beads) were derived from  $NVT$  MD interaction energies as described by us in previous reports.<sup>40,41</sup> Shortly, the interaction energy  $E_{b,\text{TFH-Au}}$  of a system composed, for instance, of THF and Au, may be derived from the corresponding simulations as:  $E_{b,\text{TFH-Au}} = E_{\text{TFH}} + E_{\text{Au}} - E_{\text{TFH}}$  in which the first two terms represent the potential energy of THF and gold, consisting of both valence and non-bonded energy terms, and the last term is the interaction energy between the two components, made up of non-bonded terms only. Next, the corresponding DPD interaction parameters  $a_{ij}$  are calculated as described in ref. 42 rescaling the relative MD interaction energies.

**Table 2** DPD interaction parameters  $a_{ij}r_c/k_B T$  employed in this work

	PS	PVP	Au	Solvent
PS	25.0			
PVP	$\frac{a_{\text{PVP-PS}}r_c}{k_B T}$	24.1		
Au	29.8	26.2	23.0	
THF	26.1	26.4	32.1	25.0

**Table 3** DPD interaction parameter  $a_{\text{PVP-PS}}$  for diblock copolymer chains of chain length  $N$

$N$	$\frac{a_{\text{PVP-PS}}r_c}{k_B T}$
4	44.7
8	40.8
12	39.1
16	38.1
20	37.4
24	36.9
28	36.6

All DPD interaction parameters employed in this work are summarized in Table 2. The DPD interaction parameters for DBCs as a function of the total chain length  $N$  are reported in Table 3.

### Simulation details

All simulation trajectories were generated employing the GNU simulation software DL\_MESO<sup>44</sup> suitable for parallel DPD simulations. Equations of motion were integrated with the velocity Verlet algorithm with a reduced time step  $\Delta t = 0.03$  to avoid fluctuations in the shape of Au NPs. We adopted standard DPD units, where  $r_c$  is a unit of length,  $k_B T$  is a unit of energy and, since PS and PVP monomers have almost identical molar mass, we set both PS and PVP bead mass to unity. The reduced density was fixed to  $\rho r_c^3 = 3$ , except for the NP core for which higher density was assigned to avoid penetration of either polymers or solvent beads.

All simulations started from initial configurations where one polymer-grafted NP was placed in the middle of a simulation box. Polymer chains were grafted radially onto the surface of NP by one end. In the case of DBC, the PVP block was grafted to the NP while the PS block constituted the chain free end.

A  $20r_c \times 20r_c \times 20r_c$  simulation box was used for grafted chains up to  $N = 12$  while a  $30r_c \times 30r_c \times 30r_c$  simulation box was adopted for longer chains. To avoid finite size effects (*i.e.*, interaction of the NPs with its periodic images), the distribution of the solvent from the center of mass (COM) of the NP was predicted in preliminary simulation runs (see Fig. S1, ESI†). The distance at which the solvent reaches its maximum (*i.e.*, the distance at which it is not perturbed by the presence of the NP and achieves its bulk value) represents the minimal length (referred to as the COM of the NP) required to eliminate artificial particle interactions. Accordingly, this length was adopted to set the simulation box size.

Each initial configuration was first equilibrated for  $1 \times 10^6$  time steps. Then,  $1 \times 10^4$  uncorrelated configurations

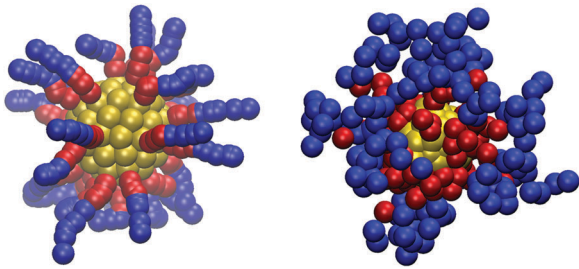


Fig. 1 DPD snapshots for the initial (left) and equilibrated (right) structure of the PVP<sub>3</sub>PS<sub>5</sub> grafted nanoparticle. Legend: PS, blue; PVP, red; Au, yellow. Solvent beads are not shown for clarity.

were collected during additional  $2 \times 10^6$  time steps to calculate ensemble averages. Fig. 1 shows the initial (left) and final (right) configuration for the PVP<sub>3</sub>PS<sub>5</sub> system.

Details about statistics and correlation analysis are given in the ESI.†

## Results and discussion

In this work we employed DPD to systematically investigate the structure and scaling behavior of PVP<sub>*n*</sub>PS<sub>*m*</sub> DBCs of different chain lengths and relative composition grafted on the surface of gold NP.

First, a validation of the proposed DPD models was performed by predicting the scaling behavior and the brush thickness of Au NPs grafted with PS homopolymer ligands, for which a theoretical framework and experimental evidence<sup>39</sup> is available for comparison.

Once the proposed model was validated, we explored the effect of the chain length and architecture on the characteristics of the spherical NP grafted DBCs.

From a theoretical standpoint, it is known that, when the size of the grafted homopolymer chain exceeds the size of the NP core, the chain scaling behavior can be described by the Daoud–Cotton model for star polymers.<sup>20</sup> In this theory, the radial monomer density profile of a star polymer is captured through scaling arguments that suggest the presence of up to three separate asymptotic regions: a dense core where the radial monomer density is constant, an “unswollen” region where local density effects screen out excluded volume interactions leading to behaviour reminiscent of  $\theta$ -solvent scaling, and a “swollen” region where spatial dilation provides enough room for excluded volumes to enforce self-avoiding walk (or good solvent) behaviour. It was shown earlier<sup>23,45</sup> that scaling behavior of spherical brushes can be described by the DC model in the limit of long chains and if the number of grafted chains  $G \gg 1$  (a full description of scaling functions for the structural properties of spherical brushes in the DC framework can be found in the ESI†).

The simulation results for the brush height ( $H$ ) and monomer number density profiles ( $\phi(r)$ ) for the PS homopolymer with a chain of length equal to  $N = \{4, 8, 12, 16, 20, 24, 28\}$  are displayed in Fig. 2 and 3. The mean end-to-end distance ( $R_e$ ), the mean square radius of gyration ( $R_g^2$ ) and end-monomer

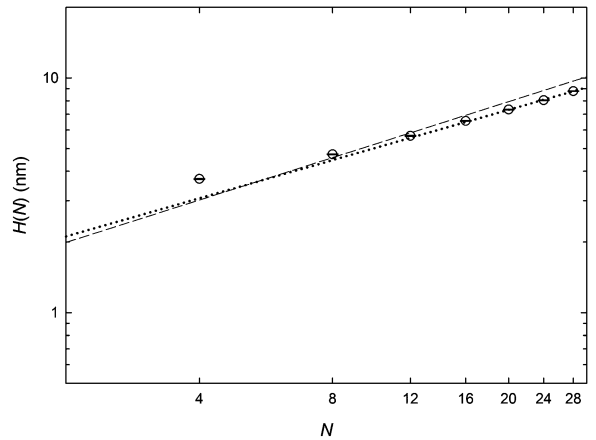


Fig. 2 Brush height  $H(N)$  obtained as a maximum of a Weibull distribution for different chain lengths  $N$ . The dotted line represents the scaling of  $H(N)$  while the scaling of the Daoud–Cotton model is shown as a dashed line for comparison.

number density ( $\phi_{\text{end}}(r)$ ) for the above systems are provided in Fig. S2–S4, respectively, of the ESI.†

According to the DC model,  $R_e$ ,  $H$  and  $R_g^2$  data were fitted only to those chains whose length exceeds the size of the nanoparticles. Thus, given the  $R_g$  values of PS homopolymers listed in Table S2 (ESI†), we typically fitted data for chains with  $N \geq 16$ . Finally, the behavior of  $R_e$  and  $H$  was fitted to:

$$R_e = H = \alpha G^{\frac{1-A}{2}} N^A \quad (12)$$

while for  $R_g^2$  we employed the relationship:

$$R_g^2 = \alpha G^{1-A} N^{2A} \quad (13)$$

Monomer density profiles  $\phi$  were fitted to:

$$\phi(r) \approx \begin{cases} \beta G^{1/2} r^{-1} & \text{inner part of the profile} \\ \gamma G^{2/3} r^{-4/3} & \text{outer part of the profile} \end{cases} \quad (14)$$

In the above equations,  $r$  is the distance from the center of mass of the nanoparticle, and  $\alpha$ ,  $\beta$ ,  $\gamma$ , and  $A$  are the corresponding scaling coefficients, where for  $A$  the DC model predicts the Flory value of  $3/5$ .

The values of scaling coefficients for the different PS homopolymer chains are summarized in the second row of Table 4.

Very good agreement of the scaling behavior of  $R_e$  and  $R_g^2$  is observed in our benchmark simulations of Au NP grafted by the PS homopolymer. The scaling coefficients  $A = 0.65 \pm 0.01$  for  $R_e$  and  $A = 0.59 \pm 0.02$  for  $R_g^2$  obtained in our simulations are very close to the Flory value of 0.6 used in the DC model. Scaling of  $R_e$  and  $R_g^2$  is further detailed in Fig. S2 and S3 of the ESI.†

Pleasantly, the comparison of available experimental evidence of the PS brush thickness  $H(N)$  anchored onto 3 nm sized Au gold NPs dispersed in a dilute solution of good solvent showed very good agreement with our simulation predictions; thus, in the case of PS chains with  $N = 4$  we estimated a brush height of 1.83 nm (Fig. 2), with the experimental counterpart being 2.03 nm.<sup>31</sup> Contextually, we expected<sup>31</sup> a brush thickness

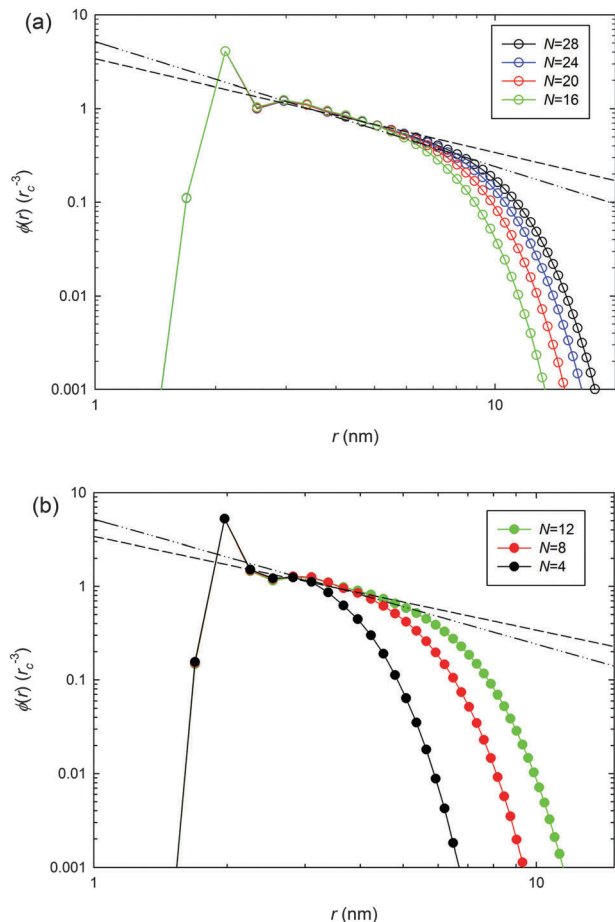


**Fig. 3** Log–log plot of PS monomer number density profiles  $\phi(r)$  measured from the center-of-mass of the NP for PS homopolymers grafted onto spherical Au NPs. The solid line serves as a guide to the eye. (a) Monomer density profiles  $\phi(r)$  for long PS homopolymer chains ( $N \geq 16$ ). (b) Monomer density profiles  $\phi(r)$  for short PS homopolymer chains. The dashed line represents the scaling of the inner part of the profile, while the dash-dotted line corresponds to the scaling of the outer part of the density profile. Scaling behavior was fitted for the longest chain in our simulation, *i.e.*  $N = 28$ .

**Table 4** Scaling coefficients of the mean end-to end distance  $R_e$ , mean square radius of gyration  $R_g^2$ , brush height  $H(N)$  and monomer density profile  $\phi(r)$  for spherical Au nanoparticle grafted by PS, PVP homopolymers or by symmetric PVP<sub>*n*</sub>PS<sub>*n*</sub> diblock copolymer. Simulation uncertainties are given in the last digit as subscripts. Flory values used by the Daoud–Cotton model predict  $A = 0.6^{20}$

	$R_e$ (nm)	$R_g^2$ (nm <sup>2</sup> )	$H(N)$ (nm)	$\phi(r)$
PS	$\alpha = 0.63_5$ $A = 0.65_1$	$\alpha = 0.07_7$ $A = 0.59_2$	$\alpha = 0.65_4$ $A = 0.55_4$	$\beta = 0.44_1$ $\gamma = 0.36_3$
PVP	$\alpha = 0.61_7$ $A = 0.64_1$	$\alpha = 0.06_6$ $A = 0.59_1$	$\alpha = 0.61_5$ $A = 0.55_6$	$\beta = 0.44_1$ $\gamma = 0.36_3$
PVP <sub><i>n</i></sub> PS <sub><i>n</i></sub>	$\alpha = 0.71_2$ $A = 0.63_2$	$\alpha = 0.06_1$ $A = 0.58_6$	$\alpha = 0.61_6$ $A = 0.49_1$	$\beta = 0.43_5$ $\gamma = 0.32_2$

of 4.4 nm for PS homopolymer chains of  $N = 14$  and the value of 4.9 nm was found in our calculations (Fig. 2).

Fig. 3 shows monomer density profiles obtained from the center-of-mass of the nanoparticle for the NP-grafted PS

homopolymer chains. The DC model describes two important scaling regimes for the monomer density profile: first, the high density of polymer segments near surface of the NP screens out the excluded volume effects, and the monomer density profile scales as  $G^{1/2}r^{-1}$ . Then, moving away from the surface of the NP, the excluded volume effects change the scaling of the monomer density profile to  $G^{2/3}r^{-4/3}$ . The first pronounced peak in the density profiles stems from the first stiff bond between the first polymer bead and the surface of the Au NP and was observed also in other simulation studies.<sup>23,24</sup> The region of high concentration of PS polymer beads is established for longer chains in our systems, as shown in Fig. 3a, where the relevant scaling agrees very well with the DC model. Nevertheless, the region with excluded volume effects is very small due to the soft nature of the interaction potential between the polymer and the solvent. For short polymer chains (Fig. 3b), the region with high concentration of polymers is reduced, and the region with excluded volume effects is no longer detected. Furthermore, for  $N = 4$  we see that the decay of the relevant monomer density profile is similar to the parabolic decay observed for flat planar brushes.<sup>23,45</sup>

As expected, the same analysis applied to simulations performed with PVP homopolymers as grafted chains reveals that the scaling behavior of PVP homopolymers is utterly similar to the one exhibited by PS homopolymers (compare scaling coefficients in Table 4 and Fig. S5–S7, ESI†). Nevertheless, higher attractive interactions between the PVP segments and the Au NP tend to reduce the size of the polymer shell, *i.e.*, to reduce the value of the brush height  $H(N)$  (see ESI† for more results).

Simulation results for PS and PVP homopolymers grafted on the surface of spherical Au NPs proved that our DPD model is able to properly capture the structure and scaling behavior of these polymer-grafted NPs.

Next, we went on extending the prediction to PVP<sub>*n*</sub>PS<sub>*m*</sub> DBC chains. These offer additional parameters with respect to homopolymers to fine-tune and control the brush behavior. Thus, understanding the influence of the block sequence and the chain length is instrumental in tailoring polymer-modified NP surface properties.

For this purpose, we adopted the same chain lengths employed for homopolymers, *i.e.* the total length of the DBC chain varied to be  $N = \{4, 8, 12, 16, 20, 24, 28\}$ . In addition, for each chain length we modeled several different chain compositions by varying the PVP block length ratio,  $f_{\text{PVP}}$  (see Table 1). In its original formulation, the DC model does not consider the effect of chemical incompatibility between different blocks in a DBC chain. Therefore, the comparison of scaling behavior of symmetric DBCs with scaling of the DC model is more qualitative than quantitative. Accordingly, upon discussing our results for DBC chains we rather focused on the effect of the chain architecture on monomer distribution, the distribution of chain free-ends, and the size of the polymer shell.

The scaling behavior for  $R_e$  and  $R_g^2$  of Au spherical NPs decorated with symmetric DBC,  $f_{\text{PVP}} = 0.5$  is shown in Fig. 4a and b, respectively. As before, we fit data only for chains for which the size of the chain exceeds Au NP dimensions (*i.e.*,  $N \geq 16$  beads, Table S2, ESI†).

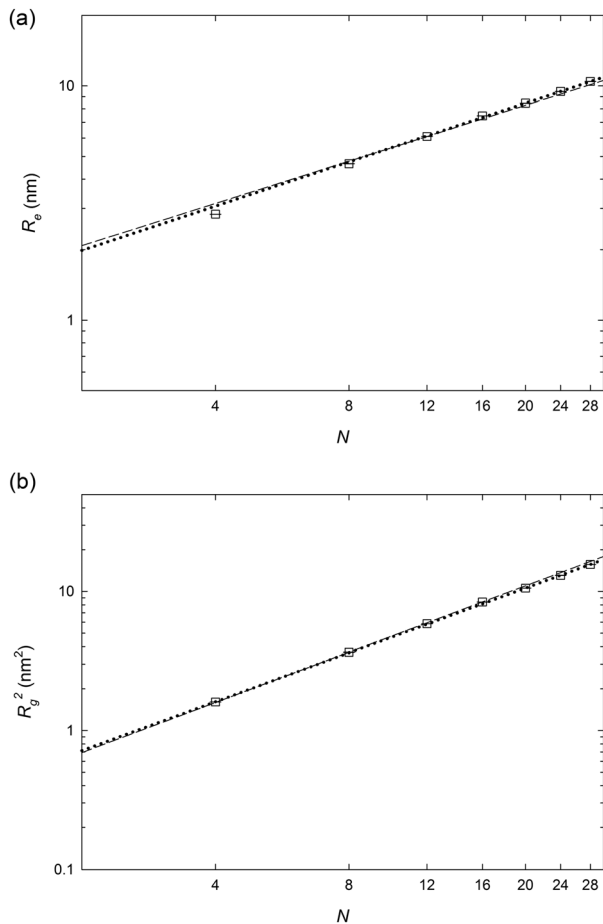


Fig. 4 Log-log plot of (a) end-to-end distance  $R_e$  and (b) mean square radius of gyration  $R_g^2$  of the symmetric  $\text{PVP}_n\text{PS}_m$  diblock copolymer grafted onto spherical Au NPs. Dotted lines represent the scaling of  $R_e$  and  $R_g^2$  obtained for long polymer chains ( $N > 16$ ) while dashed lines show the scaling of the Daoud-Cotton model for comparison.

From our results we see that interactions between  $\text{PVP}_n$  and  $\text{PS}_m$  blocks do not influence the scaling of single chain properties as the scaling coefficients in Table 4 are very close to the scaling coefficients obtained for homopolymers. In contrast, the repulsion between  $\text{PVP}_n$  and  $\text{PS}_m$  blocks modifies the radius of gyration  $R_g^2$  and the shape of the end-monomer distribution  $\varphi_{\text{end}}(r)$ , as shown in Table S2 (ESI<sup>†</sup>) and Fig. 5a, respectively, from which we see that, in contrast to the case of PS homopolymers, more chain ends are distributed throughout the polymer shell instead of being located only in the outer part of the shell (as expected from the DC model), and the curvature of  $\varphi_{\text{end}}(r)$  is more pronounced. For comparison, the shape of  $\varphi_{\text{end}}(r)$  for the PS homopolymer in Fig. S4 (ESI<sup>†</sup>) indicates that more chain ends are located in the outer part of polymer shell. Moreover, the scaling behavior of the brush height  $H(N)$  in Fig. 5b does not follow the scaling predicted by the DC model, and the scaling coefficients in Table 4 being smaller.

In addition, the overall distribution of monomers  $\phi(r)$  obtained is displayed in Fig. 6a for long chains and in Fig. 6b for short chains, respectively. As is apparent from the graphs, the interactions between  $\text{PVP}_n$  and  $\text{PS}_m$  blocks suppressed the

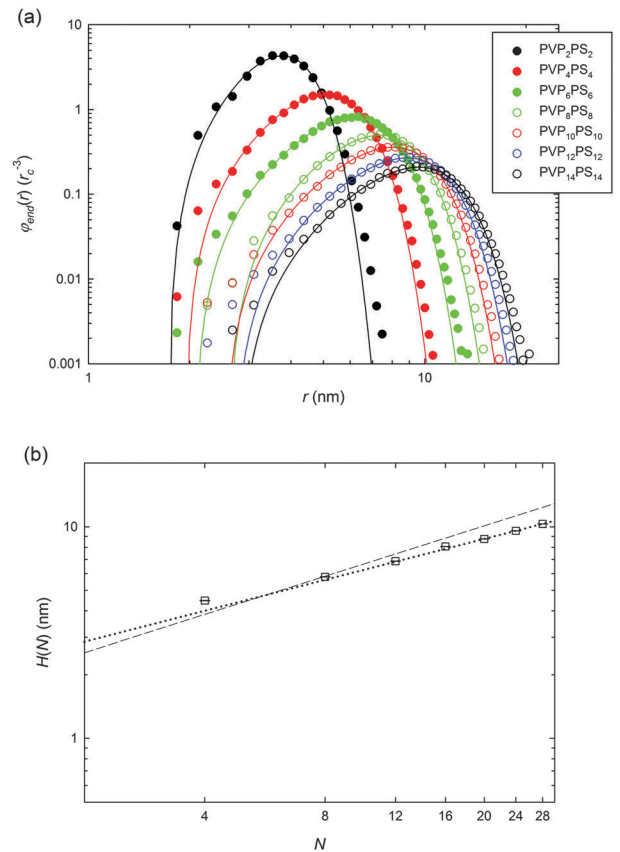


Fig. 5 Log-log plot of the (a) end monomer number distribution  $\varphi_{\text{end}}(r)$  and (b) brush height  $H(N)$  for symmetric  $\text{PVP}_n\text{PS}_n$  DBCs grafted onto spherical Au NPs. In panel (b), the dotted line represents the scaling of  $H(N)$  obtained for long polymer chains ( $N > 16$ ) while the scaling of the Daoud-Cotton model is shown as a dashed line for comparison.

effect of the first stiff bonding observed for the PS homopolymer in Fig. 3, and the relevant peak is much less pronounced. From Fig. 6a, we also see that the region with high concentration of polymer beads (*i.e.*, the inner region) is reduced and the region with the excluded volume effect (*i.e.*, the outer region) is established. Nevertheless, the presence of the outer region stems from the interactions between  $\text{PVP}_n$  and  $\text{PS}_m$  blocks and not from the explicit incorporation of excluded volume interactions due to the soft nature of our potential. In Fig. 6b, the establishment of the inner and outer regions for short chains, with the exception of the shortest chain with  $N = 4$  beads, is evident. The strong repulsion between the  $\text{PVP}_n$  and  $\text{PS}_m$  blocks expands the inner region of the shortest chain, although the size of the chain is still smaller than the size of the NP.

Fig. 7 shows the partial monomer number density per chain for PS and PVP blocks as a function of the distance from the COM of the nanoparticle for symmetric DBC and chain lengths  $N = 8, 16$  and  $24$ , chosen as representative systems. The curves of PS and PVP beads (full and empty black circles in Fig. 7) indicate that un-grafted PS blocks are folded inside the brush, exhibiting some lateral segregation, but without specific ordering. In neutral solvents the folding of the PS chain is related to

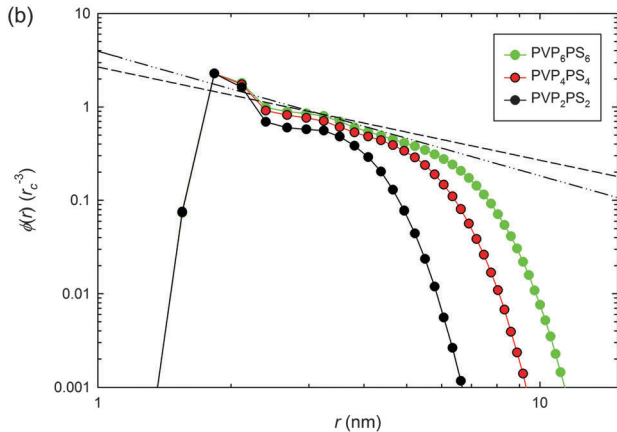
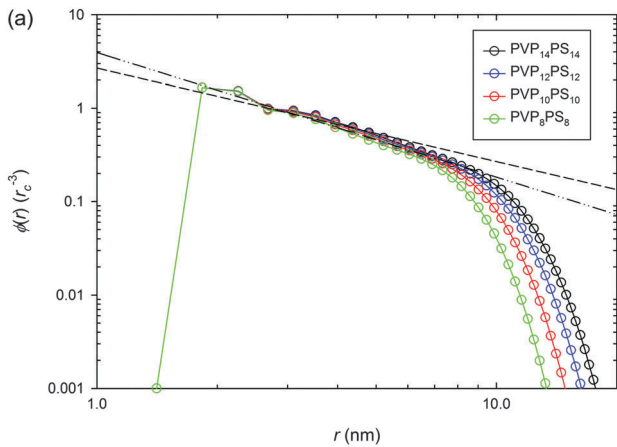


Fig. 6 Log-log plot of monomer number density profiles  $\phi(r)$  for the symmetric  $\text{PVP}_n\text{PS}_n$  DBC chain grafted onto Au NPs. measured from the center-of-mass of Au nanoparticles. The solid line serves as a guide to the eye. (a) Monomer density profiles  $\phi(r)$  for long diblock chains ( $N \geq 16$ ). (b) Monomer density profiles  $\phi(r)$  for short diblock chains. The dashed lines represent scaling of the inner part of the profile, while dash-dotted lines correspond to scaling of the outer part of the density profile. Scaling behavior was fitted for the longest chain in our simulation, *i.e.*  $N = 28$ .

the chain conformational entropy instead of solvent selectivity. The described behavior was observed also experimentally for sufficiently large grafting density and/or high block incompatibility in nonselective good solvents of PS-*b*-PMA brushes on flat substrates.<sup>46</sup> Moreover, the corresponding homopolymer PS and PVP profiles (green empty circles and filled red circles, respectively, in Fig. 7) are shifted more towards the surface of the Au NP, thus reflecting the repulsive nature between PS and PVP blocks in the DBC chain. Figures for all chain lengths of symmetric DBC considered in this work are shown in ESI†, Fig. S8.

To elucidate more the composition of the copolymer shell we followed the approach proposed by Meng *et al.*<sup>47</sup> to measure the contribution of the PS, and PVP beads on the composition of the surface layer  $\phi_i^{\text{SL}}(H)$  calculated as:

$$\phi_i^{\text{SL}}(H) = \frac{\int_H^r \phi_i(r) dr}{\int_H^r \phi(r) dr} \quad (15)$$

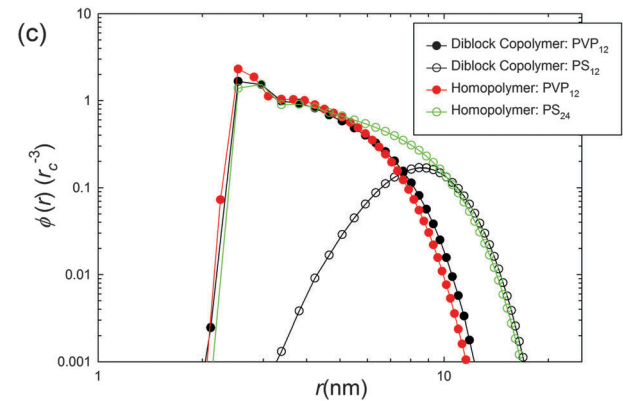
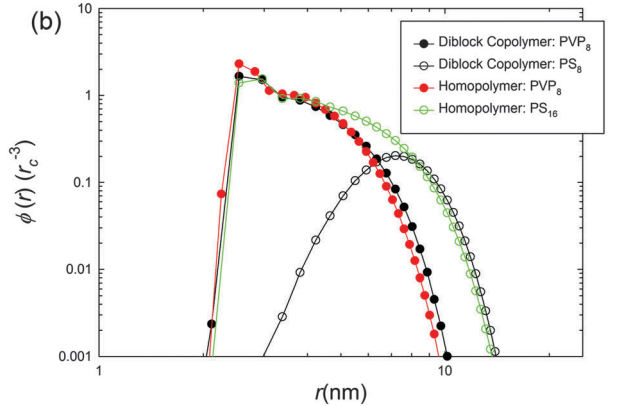
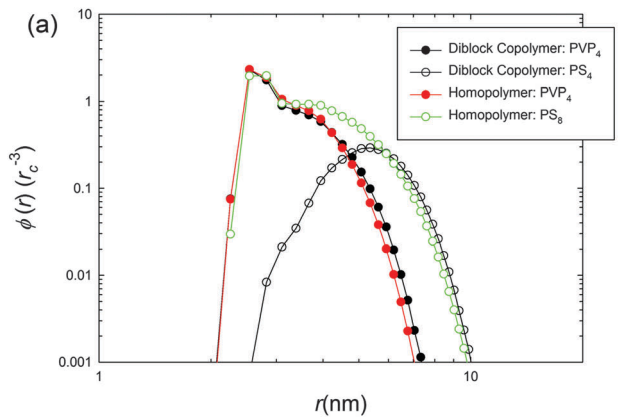


Fig. 7 Log-log plot of monomer number density profiles  $\phi(r)$  for (a)  $\text{PVP}_4\text{PS}_4$ , (b)  $\text{PVP}_8\text{PS}_8$  and (c)  $\text{PVP}_{12}\text{PS}_{12}$  symmetric DBC chain. Full black/red circles show density profiles of  $\text{PVP}_n$  beads in diblock copolymers and homopolymer chains, respectively; empty white/green symbols show  $\text{PS}_n$  beads, in diblock copolymers and homopolymer chains, respectively.

where  $\phi_i(r)$  is the number density of the block  $i$  (PS or PVP) and  $\phi(r)$  is the total number density of both blocks at a distance  $r$  from the COM of the nanoparticle (at  $r > H$ ). As defined, the surface layer composition  $\phi_i^{\text{SL}}(H)$  is measured by the distance from the COM of the NP corresponding to the brush height  $H$  up to the end of the corresponding density profiles. The values for  $\phi_{\text{PS}}^{\text{SL}}(H)$  and  $\phi_{\text{PVP}}^{\text{SL}}(H)$  in symmetric DBCs are reported in Fig. 8. As can be seen, the surface layer is always formed mostly by PS beads, while PVP beads, bonded to the surface of the Au NP, contribute only marginally. Moreover, the values for  $\phi_{\text{PS},H}$

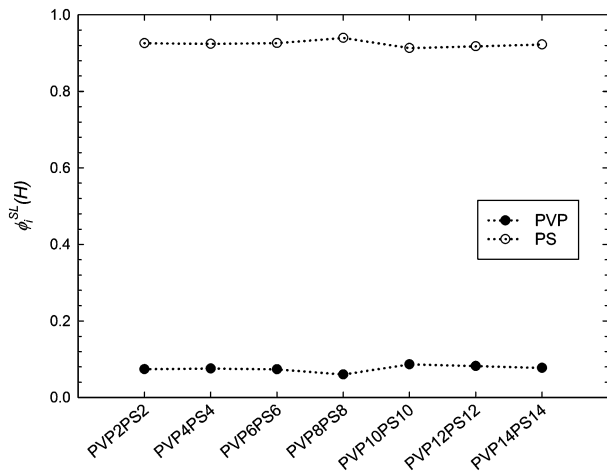


Fig. 8 Effect of the chain length  $N$  on the surface layer composition  $\phi_i^{\text{SL}}(H)$  of symmetric DBCs. Dotted lines serve as a guide to the eye.

and  $\phi_{\text{PVP,H}}$  in symmetric DBCs are very similar, indicating that the copolymer chain length  $N$  has only a weak influence on the surface composition.

Furthermore, by varying the PVP block length ratio  $f_{\text{PVP}}$ , we investigated the effect of chain composition on chain and polymer shell properties (Fig. 9). The effect of chain composition for a DBC with  $N = 12$  is reported in Fig. 9a and b as an example.

In detail, from the end-monomer distribution  $\varphi_{\text{end}}(r)$  in Fig. 9a we see that, by increasing the length of the PVP block bonded to the surface of the Au NP, the repulsion between blocks shifts the position of the maxima in  $\varphi_{\text{end}}(r)$  away from the NP surface, see also Fig. 7. Therefore, the size of the chain, expressed as the end-to-end distance  $R_e$ , increases up to symmetric DBC,  $f_{\text{PVP}} = 0.5$  (Fig. 9b). When the length of the PVP block is dominant, the chain behaves more like a homopolymer (behavior captured also in Fig. 10). This effect is further presented and summarized in terms of brush height  $H(N)$  as a function of  $f_{\text{PVP}}$ , for chains with  $N \leq 20$  beads (Fig. 9c).

The effect of chain architecture,  $f_{\text{PVP}}$ , on PS and PVP monomer density profiles is illustrated in Fig. 10 for four different DBC compositions and total chain length  $N = 12$ . Profiles of all chain architectures considered in this work are reported in the ESI†, Fig. S9.

Modifying  $f_{\text{PVP}}$  from 0.08 up to 0.92, the shape of  $\text{PVP}_m$  distribution radically changes. This originates from the first stiff bond between the PVP bead and the surface gold bead. The shape of  $\phi(r)$  for  $\text{PS}_n$  is very similar for all chain compositions, where the deviation of the profile from the parabolic shape stems from the favorable influence of gold surface beads. Red curves in Fig. 10 represent the monomer density profiles for the corresponding PVP homopolymers. We notice that the effect of the additional interaction between PS and PVP blocks is less pronounced as the DBC chain becomes more PVP like. Curves of PVP homopolymers and the PVP part of the diblock copolymer nearly coincide in Fig. 10d, where the DBC chain is composed mainly of PVP beads. Moreover, as seen previously,

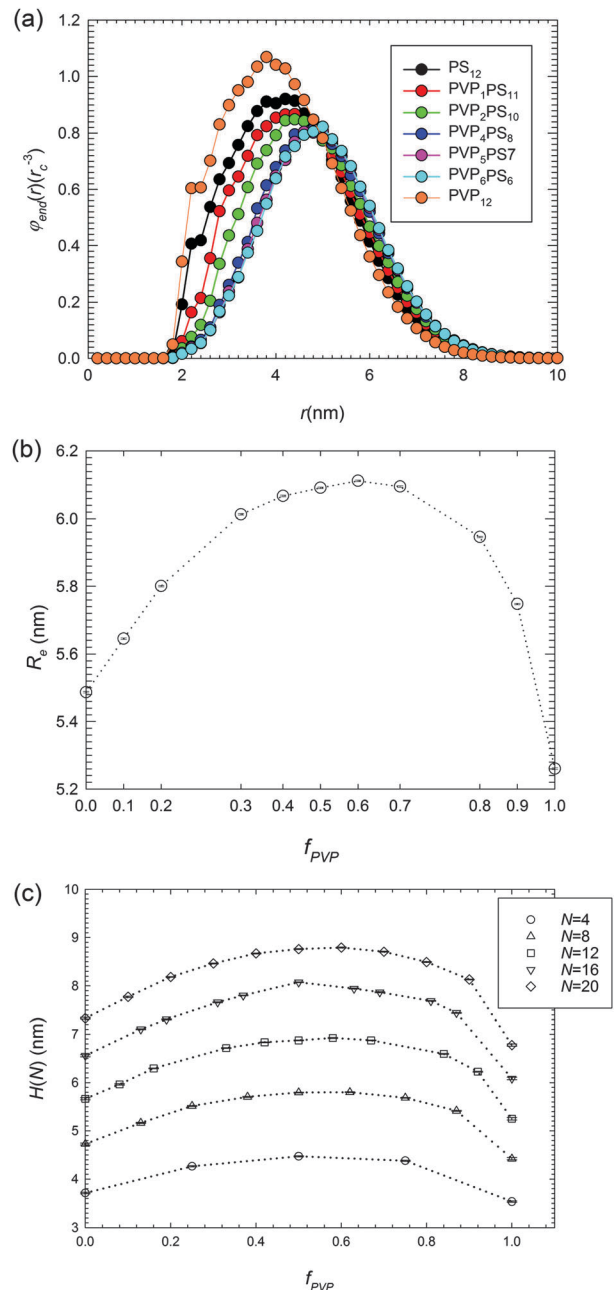


Fig. 9 (a) Effect of chain composition on the end-monomer number distribution  $\varphi_{\text{end}}(r)$ , and (b) end-to-end distance  $R_e$  of DBC chains with  $N = 12$  grafted onto Au NPs. (c) Brush height  $H(N)$  for DBCs with different chain lengths  $N$  and different relative block composition ( $f_{\text{PVP}}$ ). Solid and dotted lines are guide to the eye.

the un-grafted PS blocks are embedded inside the corona, regardless of the chain composition and lateral separation occurs.

The surface layer composition, measured from the brush height  $H$  up to the end of the PS/PVP density profile (eqn (15)), is reported in Fig. 11 for the DBC chain with  $N = 12$  as a function of chain composition  $f_{\text{PVP}}$ . For  $f_{\text{PVP}}$  less than 0.5, the nanoparticle external layer is mainly constituted by PS segments. At  $f_{\text{PVP}}$  values around 0.72 we see a breakeven point and

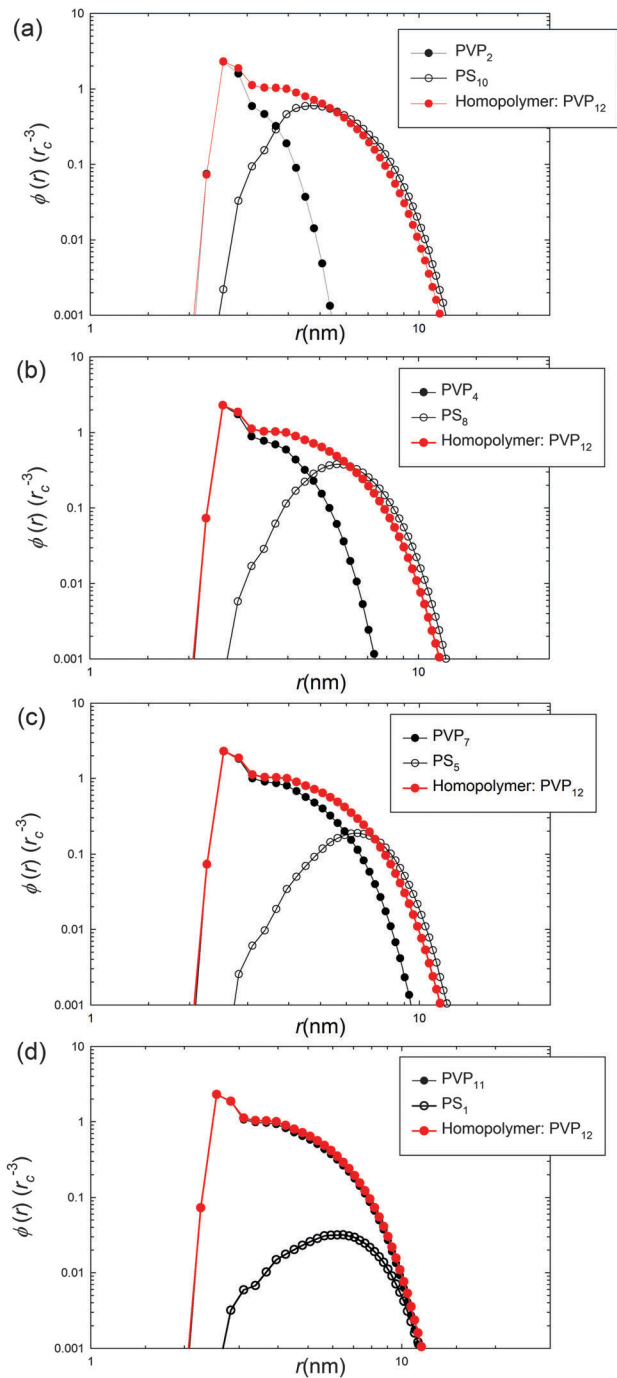


Fig. 10 Log-log plot of monomer number density profiles  $\phi(r)$  for DBC chain with  $N = n + m = 12$  beads. (a)  $\text{PVP}_2\text{PS}_{10}$ , (b)  $\text{PVP}_4\text{PS}_8$ , (c)  $\text{PVP}_7\text{PS}_5$  and (d)  $\text{PVP}_{11}\text{PS}_1$ . Full circles shows monomer density profiles of  $\text{PVP}_m$  beads and empty symbols shows  $\text{PS}_n$  beads. Red curves indicate monomer density profiles for the corresponding PVP homopolymer.

the surface is equally made by PS and PVP blocks. Finally, when  $f_{\text{PVP}}$  exceeds 0.8, the presence of PS blocks dramatically decreases. This was observed for all chain lengths analyzed (Fig. S10, ESI<sup>†</sup>), thereby confirming that  $N$  is a weak parameter in controlling the nanoparticle shell composition. More likely, the surface layer is controlled by chain composition, interaction

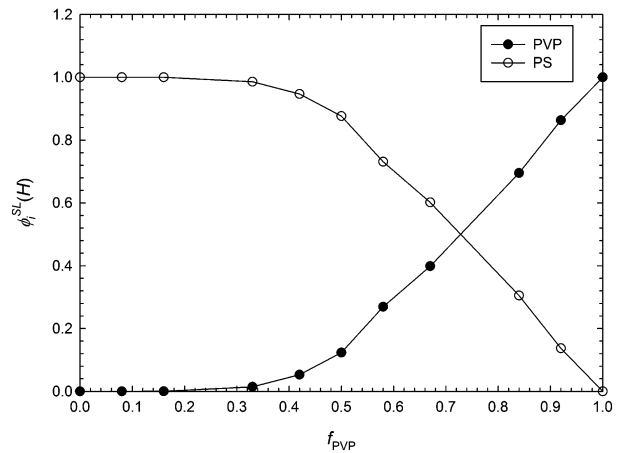


Fig. 11 Effect of the architecture ( $f_{\text{PVP}}$ ) on the surface layer composition  $\phi_i^{\text{SL}}(H)$  of a DBC of total length  $N = 12$ .

of PS and PVP beads, and grafting density with the surface of the Au nanoparticle (see additional data in Fig. S11, ESI<sup>†</sup>). On the other hand, this constitutes an extremely interesting result from a practical standpoint, since varying the percentage of the blocks is an easy way to tailor the decorated-nanoparticle surface characteristics.

## Conclusions

The aim of this study was to thoroughly investigate the scaling law behavior and structural features of PS/PVP polymer brushes grafted onto Au nanoparticles under good solvent conditions using theory and DPD simulations. Accordingly, homopolymer and diblock copolymer chains were both considered, and the influence of chain length and block composition on structural parameters and the scaling behavior was discussed in detail. Importantly, the model adopted in the present work can treat length scales accessible to real systems, allowing for direct comparison with experimental findings.

In summary, a good agreement between the DC theory and our DPD model for Au spherical NPs grafted either by PS or PVP homopolymers brushes was observed in the scaling behavior of single chain properties (*i.e.*,  $R_c$  and  $R_g^2$ ), especially for long chains ( $N \geq 16$ ).

We showed that, when polymers and NPs have comparable dimensions, the shape of the monomer density profile  $\phi(r)$  is comparable to parabolic decay observed for flat brushes. Moreover, the shape of the end-monomer distribution  $\phi_{\text{end}}(r)$  has a pronounced curvature as well and deviates from the scaling behavior of the brush height of longer chains, whose scaling behavior compares rather well with the DC model. Furthermore, a region of high concentration of polymer segments was observed in the monomer density distribution for long homopolymers. Nevertheless, the region with excluded volume interactions is rather small due to the soft interactions between the polymer and the solvent. The region with a high concentration of polymer beads is further reduced, and the region of excluded volume interactions is even suppressed for short polymers. For

the PS homopolymer with  $N = 4$  we obtained a parabolic decay of the monomer distribution, similar to what is observed for flat planar brushes.

The repulsion between PS and PVP in block copolymers was found to influence the radius of gyration and the shape of the end-monomer distribution (*i.e.* the static properties) of the polymer shell. Moreover, for diblock chains the un-swollen region was thinner (and the swollen layer thicker) than that of the homopolymer of the same length.

Lateral segregation was found to occur regardless of the chain length and composition due to the high grafting density considered for these systems. Interestingly, the total chain length affects the surface composition of the polymer brush only weakly, while the chain architecture plays a substantial role.

A polymer brush layer grafted on the surface protects the stability of the particle, at the same time providing a diverse number of applications for these systems depending on the responsiveness of the NP decorating brush.

However, notwithstanding the vast array of different applications that can be envisaged for copolymer-grafted nanoparticles, their systematic study still lags behind those concerning their homopolymer-functionalized counterparts. Therefore, given the enormous and highly time-consuming efforts required to conduct systematic parametric studies for DBC-modified NPs, we expect that the results reported in the present work will provide practical guidelines to the design of smart NP surfaces with diblock copolymer brushes tailored for specific targeted applications.

## Acknowledgements

ZL and ML acknowledge support by the Czech Science Foundation (Project No. P106-13-02938S), by the Internal Grant Agency of J. E. Purkinje University (Project No. 53224 15 0005 01), and by the Grant Program of the Ministry of Education, Youth and Sports (Project No. LH12020). The computer time was provided by the METACentrum computing facility and by the HPC cluster ENPUTRON.

## References

- 1 J. Kao, K. Thorkelsson, P. Bai, B. J. Rancatore and T. Xu, *Chem. Soc. Rev.*, 2013, **42**, 2654–2678.
- 2 B. Zhao and L. Zhu, *Macromolecules*, 2009, **42**, 9369–9383.
- 3 Y. Chen, *Macromolecules*, 2012, **45**, 2619–2631.
- 4 M. G. Moffitt, *J. Phys. Chem. Lett.*, 2013, **4**, 3654–3666.
- 5 B. Jaquet, D. Wei, B. Reck, F. Reinhold, X. Zhang, H. Wu and M. Morbidelli, *Colloid Polym. Sci.*, 2013, **291**, 1659–1667.
- 6 S. K. Kumar, N. Jouault, B. Benicewicz and T. Neely, *Macromolecules*, 2013, **46**, 3199–3214.
- 7 P. Akcora, H. Liu, S. K. Kumar, J. Moll, Y. Li, B. C. Benicewicz, L. S. Schadler, D. Acehan, A. Z. Panagiotopoulos, V. Pryamitsyn, V. Ganesan, J. Ilavsky, P. Thiyagarajan, R. H. Colby and J. F. Douglas, *Nat. Mater.*, 2009, **8**, 354–359.
- 8 E. W. Edwards, M. Chanana, D. Wang and H. Möhwald, *Angew. Chem., Int. Ed.*, 2008, **47**, 320–323.
- 9 P. Tiwari, K. Vig, V. Dennis and S. Singh, *Nanomaterials*, 2011, **1**, 31–63.
- 10 B. Lego, M. Franois, W. G. Skene and S. Giasson, *Langmuir*, 2009, **25**, 5313–5321.
- 11 J. R. Ell, D. E. Mulder, R. Faller, T. E. Patten and T. L. Kuhl, *Macromolecules*, 2009, **42**, 9523–9527.
- 12 N. J. Fernandes, H. Koerner, E. P. Giannelis and R. A. Vaia, *MRS Commun.*, 2013, **3**, 13–29.
- 13 H. Koerner, L. F. Drummy, B. Benicewicz, Y. Li and R. A. Vaia, *ACS Macro Lett.*, 2013, **2**, 670–676.
- 14 J. Choi, C. M. Hui, M. Schmitt, J. Pietrasik, S. Margel, K. Matyjazewski and M. R. Bockstaller, *Langmuir*, 2013, **29**, 6452–6459.
- 15 Y. Jiao and P. Akcora, *Macromolecules*, 2012, **45**, 3463–3470.
- 16 X. Zhu, L. Wang, J. Lin and L. Zhang, *ACS Nano*, 2010, **4**, 4979–4988.
- 17 A. Jayaraman and K. S. Schweizer, *Langmuir*, 2008, **24**, 11119–11130.
- 18 Q. Lan, L. F. Francis and F. S. Bates, *J. Polym. Sci., Part B: Polym. Phys.*, 2007, **45**, 2284–2299.
- 19 Y.-L. Lin, C.-S. Chiou, S. K. Kumar, J.-J. Lin, Y.-J. Sheng and H.-K. Tsao, *J. Phys. Chem. C*, 2011, **115**, 5566–5577.
- 20 (a) M. Daoud and J. P. Cotton, *J. Phys.*, 1982, **43**, 531–538; (b) T. M. Birshtein and E. B. Zhulina, *Polymer*, 1984, **25**, 1453–1461; (c) E. B. Zhulina and T. M. Birshtein, *Polym. Sci. USSR*, 1986, **27**, 570–578; (d) E. Zhulina and A. C. Balazs, *Macromolecules*, 1996, **29**, 2667–2673; (e) E. B. Zhulina, T. M. Birshtein and O. V. Borisov, *Eur. Phys. J. E: Soft Matter Biol. Phys.*, 2006, **20**, 243–256.
- 21 P. Traskelin, T. L. Kuhl and R. Faller, *Phys. Chem. Chem. Phys.*, 2009, **11**, 11324–11332.
- 22 J. Zheng, L. Li, S. Chen and S. Jiang, *Langmuir*, 2004, **20**, 8931–8938.
- 23 F. Lo Verso, S. A. Egorov, A. Milchev and K. Binder, *J. Chem. Phys.*, 2010, **133**, 184901–184911.
- 24 D. I. Dimitrov, A. Milchev and K. Binder, *J. Chem. Phys.*, 2007, **127**, 084905.
- 25 A. Seifpour, P. Spicer, N. Nair and A. Jayaraman, *J. Chem. Phys.*, 2010, **132**, 164901.
- 26 T. B. Martin, A. Seifpour and A. Jayaraman, *Soft Matter*, 2011, **7**, 5952–5964.
- 27 S. Pal and C. Seidel, *Macromol. Theory Simul.*, 2006, **15**, 668–673.
- 28 J. R. Spaeth, I. G. Kevrekidis and A. Z. Panagiotopoulos, *J. Chem. Phys.*, 2011, **135**, 184903.
- 29 R. D. Groot and P. B. Warren, *J. Chem. Phys.*, 1997, **107**, 4423–4435.
- 30 P. J. Hoogerbrugge and J. M. V. A. Koelman, *Europhys. Lett.*, 1992, **19**, 155–160.
- 31 S. Ma, D. Qi, M. Xiao and R. Wang, *Soft Matter*, 2014, **10**, 9090–9097.
- 32 P. Posocco, M. Fermeglia and S. Pricl, *J. Mater. Chem.*, 2010, **20**, 7742–7753.
- 33 J.-H. Huang and X.-Z. Li, *Soft Matter*, 2012, **8**, 5881–5887.

- 34 P. He, X. Li, M. Deng, T. Chen and H. Liang, *Soft Matter*, 2010, **6**, 1539–1546.
- 35 R. Toth, F. Santese, S. P. Pereira, D. R. Nieto, S. Pricl, M. Fermeglia and P. Posocco, *J. Mater. Chem.*, 2012, **22**, 5398–5409.
- 36 A. Alexeev, W. E. Uspal and A. C. Balazs, *ACS Nano*, 2008, **2**, 1117–1122.
- 37 J. M. V. A. Koelman and P. J. Hoogerbrugge, *Europhys. Lett.*, 1993, **21**, 363.
- 38 P. Español and P. Warren, *Europhys. Lett.*, 1995, **30**, 191.
- 39 J. B. Bumjoon, J. Kim, C. J. Hawker and E. J. Kramer, *Macromolecules*, 2006, **39**, 4108–4114.
- 40 M. Maly, P. Posocco, S. Pricl and M. Fermeglia, *Ind. Eng. Chem. Res.*, 2008, **47**, 5023–5038.
- 41 P. Posocco, Z. Posel, M. Fermeglia, M. Lísal and S. Pricl, *J. Mater. Chem.*, 2010, **20**, 10511–10520.
- 42 Z. Posel, P. Posocco, M. Fermeglia, M. Lísal and S. Pricl, *Soft Matter*, 2013, **9**, 2936–2946.
- 43 M. A. Horsch, Z. Zhang, C. R. Iacovella and S. C. Glotzer, *J. Chem. Phys.*, 2004, **121**, 11455–11462.
- 44 M. A. Seaton, R. L. Anderson, S. Metz and W. Smith, *Mol. Simul.*, 2013, **39**, 796–821.
- 45 K. Binder and A. Milchev, *J. Polym. Sci., Part B: Polym. Phys.*, 2012, **50**, 1515–1555.
- 46 B. Zhao, W. J. Brittain, W. Zhou and S. Z. D. Cheng, *Macromolecules*, 2000, **33**, 8821–8827.
- 47 D. Meng and Q. Wang, *J. Chem. Phys.*, 2009, **130**, 134904.